Polymer Journal (2023) 55:829–836
https://doi.org/10.1038/s41428-023-00788-3

FOCUS REVIEW

Design of supramolecular nanosheets for drug delivery applications

Noriyuki Uchida[1,2]

Received: 6 March 2023 / Revised: 29 March 2023 / Accepted: 31 March 2023 / Published online: 9 May 2023

Abstract
Two specific concepts have emerged in the field of materials science over the last several decades: nanosheets and supramolecular polymers. More recently, supramolecular nanosheets, in which these two concepts are integrated, have attracted particular attention, and they exhibit many fascinating characteristics. This review focuses on the design and applications of supramolecular nanosheets consisting of tubulin proteins and phospholipid membranes.

Introduction

Over the past several decades, two types of materials have received significant attention in the field of materials science, namely, nanosheets and supramolecular polymers. The former are ultrathin anisotropic materials. A representative example is graphene, which was the basis of a Nobel Prize award in 2010 and exhibits remarkable electrical properties, although various nanosheet-based materials have been developed to date [1–5]. The latter consist of two-dimensional molecular assemblies [6–10] that form by precisely controlled self-assembly from simple mixtures of monomers in solution. More recently, supramolecular nanosheets that combine these two concepts (Fig. 1) have emerged in conjunction with progress in the field of nanotechnology [11–25], and various interesting functions have been reported. As an example, the two-dimensional (2D) self-assembly of DNA (so-called DNA origami) has become the basis for an important field of study by providing platforms capable of constructing a variety of complex planar nanostructures [19]. Although some supramolecular nanosheets consisting of proteins and phospholipid membranes have been developed for applications as biomaterials, specific principles for the design of such materials have not yet been established, and significant challenges remain in terms of stability and functionality. The present review summarizes the design and application of recently reported tubulin heterodimer (THD) protein-based and phospholipid membrane-based supramolecular nanosheets.

✉ Noriyuki Uchida
n-uchida@go.tuat.ac.jp

[1] Department of Applied Chemistry, Graduate School of Engineering, Tokyo University of Agriculture and Technology, 2-24-16 Naka-cho, Koganei, Tokyo 184-8588, Japan

[2] RIKEN Center for Emergent Matter Science, 2-1 Hirosawa, Wako, Saitama 351-0198, Japan

Results and Discussion

Tubulin-based nanosheets

THD is a protein that serves as a component of microtubules (MTs) found in intracellular cytoskeletons [26–33] (Fig. 2a, f). This protein is composed of α-tubulin (shown in green) and β-tubulin (shown in cream), both of which bind to guanosine triphosphate (GTP). GTP attached to the α-tubulin units can neither undergo hydrolysis into guanosine diphosphate (GDP) nor be replaced with other nucleoside phosphates. In contrast, GTP attached to the β-tubulin units can be hydrolyzed to GDP, which, in turn, can be replaced with another substituent. For example, replacement with GTP* (guanylyl 5′-α,β-methylenediphosphonate), a nonhydrolyzable GTP analog, affords THD_{GTP*}. Note that in this figure, only the nucleoside phosphates attached to β-tubulin units are included as subscripts for the sake of convenience. Both THD_{GTP} and THD_{GTP*} have been reported to self-assemble into MT_{GTP} and MT_{GTP*}, respectively, upon heating to 37 °C [26, 27]. Although MT_{GTP} depolymerizes into THD_{GDP} (Fig. 2b, g) in conjunction with the hydrolysis of bound GTP to GDP, MT_{GTP*} does not depolymerize into THD_{GDP*} because of the nonhydrolyzable nature of GTP*. Interestingly, it has been demonstrated that the coassembly of THD_{GTP} and THD_{GTP*} at a ratio of 1 to 5 (mol/mol) results in the formation of 2D

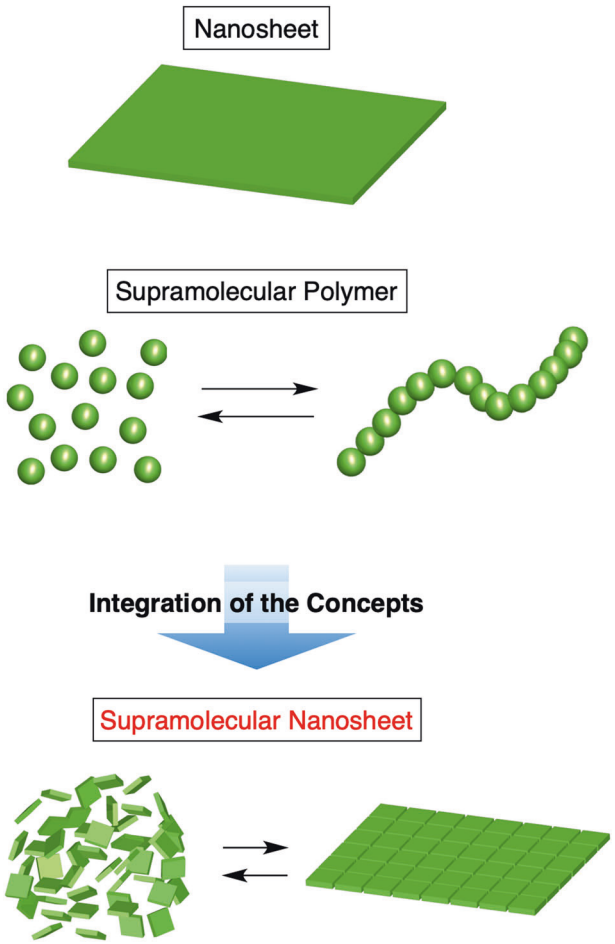

Fig. 1 Diagram showing the integration of nanosheets and supramolecular polymers to produce supramolecular nanosheets

nanosheets ($NS_{GTP/GTP*}$) rather than MTs, as confirmed by transmission electron microscopy (TEM) (Fig. 2c, h). $NS_{GTP/GTP*}$ has a leaf-like 2D structure and a thickness of approximately 5 nm, corresponding to the thickness of the THD units, as confirmed by atomic force microscopy [21]. Both MT_{GTP} and MT_{GTP*}, which are prepared from THD_{GTP} and THD_{GTP*}, respectively, are formed by the edge-closing of NS_{GTP} and NS_{GTP*}, which act as [28], and the long axis of THD_{GTP} is known to be shorter than that of THD_{GTP*} [29]. This mismatch in the size of the long axis is believed to lead to the formation of the unfolded $NS_{GTP/GTP*}$ structure rather than the folded $MT_{GTP/GTP*}$ structure. Interestingly, $NS_{GTP/GTP*}$ can transform into GTP-responsive spherical nanocapsules ($NC_{GTP/GTP*}$; Fig. 2e, i) in response to interactions with a photoreactive molecular glue ($Glue^{CO2-}$; Fig. 2d) containing multiple guanidinium ion (Gu^+) and benzophenone (BP) groups. $Glue^{CO2-}$ molecules can strongly attach to proteins under physiological conditions through the formation of multivalent salt bridges between Gu^+ ions and oxyanionic functional groups followed by photocrosslinking via BP units [21]. Molecular dynamics simulations have suggested that the adhesion of $Glue^{CO2-}$ transforms $NS_{GTP/GTP*}$ into a planar structure, resulting in the stacking and assembly of $NS_{GTP/GTP*}$ to construct spherical $NC_{GTP/GTP*}$.

GTP-responsiveness of tubulin vesicles

GTP is an intracellular molecule involved in many essential biological processes [30–37], such as cell division [33], nucleotide synthesis [34] and cell signaling [35]. During cell division, THD uses GTP as an energy source for conformational changes that induce the polymerization or depolymerization of MTs [30–32]. GTP is also a component for the self-replication of RNA viruses [38–41], such as coronaviruses. Notably, GTP is abundant in certain diseased cells (at concentrations of 1.5–4.5 mM), such as rapidly proliferating cancer cells [42] and cells infected with RNA viruses [43]. In contrast, the concentration of GTP, unlike that of adenosine triphosphate, is negligibly low in normal cells (<0.3 mM) [44]. Therefore, GTP-responsive nanocarriers could have the potential to efficiently cure cancer and to treat diseases linked to RNA viruses, including coronavirus disease 2019 (COVID-19) [41]. Interestingly, $NC_{GTP/GTP*}$ collapses upon exposure to GTP at concentrations higher than 0.5 mM (Fig. 3c, d), releasing encapsulated cargo in the process. This behavior suggests that $NC_{GTP/GTP*}$ could be used as a GTP-responsive carrier. In the presence of GTP, the GTP* in $NC_{GTP/GTP*}$ is likely to be replaced with GTP to afford NC_{GTP}, which can then collapse in association with the hydrolysis of GTP in a manner analogous to the depolymerization of MT_{GTP} (Fig. 3a). Because $NC_{GTP/GTP*}$ does not collapse in the presence of less than 0.2 mM GTP (Fig. 3b, d) and normal cells contain less than this level, GTP-responsive $NC_{GTP/GTP*}$ could be used to deliver encapsulated drug molecules solely to high-GTP regions such as cancer cells and virus-infected cells. Indeed, it has been shown that the anticancer drug doxorubicin (DOX) can be encapsulated in $NC_{GTP/GTP*}$ and administered to cancerous Hep3B cells, killing these cells more effectively than DOX without encapsulation.

Kinetically stable phospholipid nanosheets using cholic acid-based surfactants

Phospholipid assemblies such as liposomes and micelles have long been regarded as versatile biomaterials owing to their similarity to cell membranes and their high degree of biocompatibility [45, 46]. Among these, phospholipid nanosheets (sometimes referred to as bicelles) have recently attracted particular attention for the design of a variety of biomaterials. For example, phospholipid nanosheets have been found to orient themselves in relation to the strong magnetic fields applied during nuclear magnetic resonance (NMR) analyses, and membrane proteins embedded in these

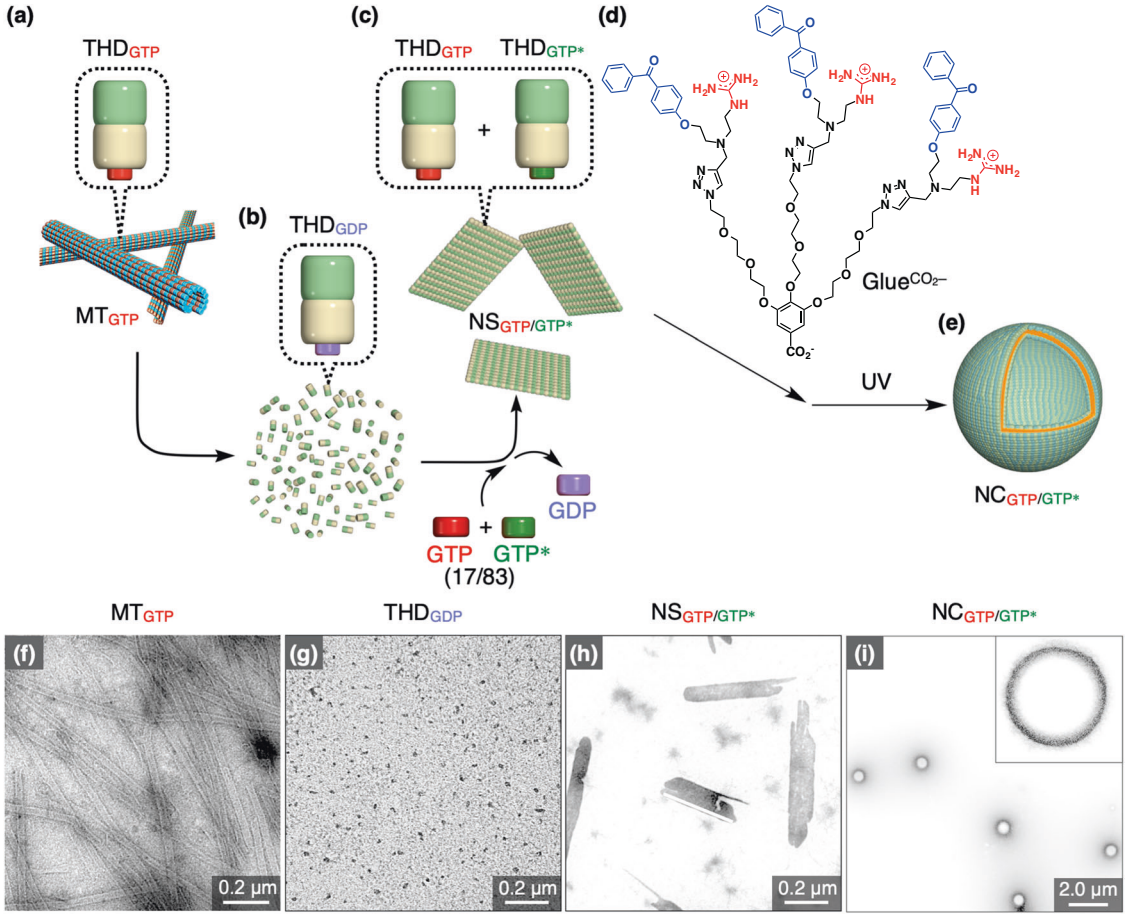

Fig. 2 Diagram summarizing the multistep procedure for the synthesis of $NC_{GTP/GTP*}$ from MT_{GTP}. In this process, (**a**) MT_{GTP} is depolymerized into (**b**) THD_{GDP}, which is subsequently incubated with a mixture of GTP* (83 mol%) and GTP (17 mol%) to form (**c**) $NS_{GTP/GTP*}$. Upon treatment with (**d**) the photoreactive molecular glue $Glue^{CO2-}$, the $NS_{GTP/GTP*}$ nanosheets are transformed into spherical (**e**) $NC_{GTP/GTP*}$. TEM images of (**f**) MT_{GTP}, (**g**) THD_{GDP}, (**h**) $NS_{GTP/GTP*}$, and (**i**) $NC_{GTP/GTP*}$

materials can provide angle-dependent NMR data that can allow structural elucidation [47]. Furthermore, it has recently been reported that phospholipid nanosheets are promising carriers for drug delivery. One advantage of these nanosheets is the extended circulation times associated with disk-shaped carriers [48] together with the stronger adhesion to microvascular networks [49, 50] compared with spherical carriers. In addition, López et al. reported that the characteristic 2D shape of phospholipid nanosheets is advantageous with regard to transdermal drug delivery applications, in which the nanocarriers need to pass through narrow gaps (6–10 nm) between skin cells [51]. The formation of phospholipid nanosheets in solution can be quantitatively evaluated by ^{31}P NMR because ^{31}P atoms in phospholipid nanosheets exhibit shifted NMR peaks that differ from those of phospholipid micelles and vesicles as a consequence of the chemical shift anisotropy of oriented ^{31}P atoms. Unfortunately, nanosheets composed of mixtures of surfactants and phospholipids typically produce unstable self-assemblies that readily transition to other morphologies in response to changes in the surrounding environment. For example, phospholipid nanosheets composed of 1,2-dimyristoyl-*sn*-glycero-3-phosphatidylcholine (DMPC) and cholic acid-based surfactants, which have been frequently studied, are known to undergo a structural transition when in dilute suspensions. This phenomenon is attributed to the phase transition temperature of DMPC ($T_m = 24$ °C), which is lower than room temperature, causing DMPC membranes to form a highly fluid liquid crystalline phase [52]. In addition, the critical micelle concentration (CMC) values of cholic acid-based surfactants are generally quite high. Hence, these surfactants easily dissociate from the edges of the phospholipid nanosheets to induce fusion of the nanosheets (Fig. 4a) [53].

Recently, phospholipid nanosheets that overcome the above problems based on the use of optimal phospholipids and surfactants have been reported [22]. One such system comprises nanosheets made of 1,2-dipalmitoyl-*sn*-glycero-3-phosphatidylcholine (DPPC, Fig. 4b) and a cholic acid-based surfactant attached to pentyl chains via a triethylene

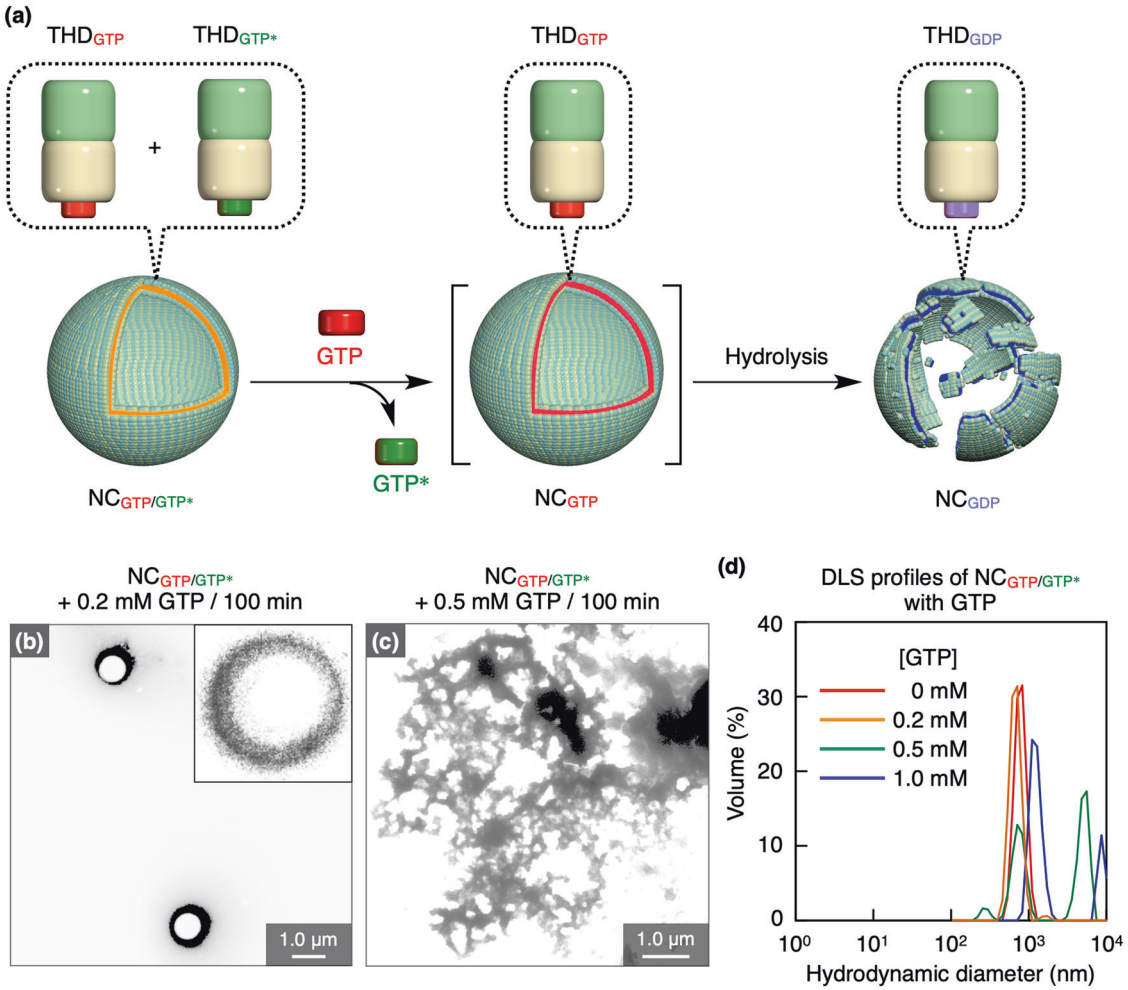

Fig. 3 **a** Diagram of the GTP-responsive collapse of $NC_{GTP/GTP*}$. TEM images of $NC_{GTP/GTP*}$ upon mixing with GTP at concentrations of (**b**) 0.2 mM and (**c**) 0.5 mM. **d** Size distribution of $NC_{GTP/GTP*}$ following titration with GTP (0–1.0 mM) as determined by DLS

glycol spacer (Chol-TEG-C_5, Fig. 4c). This material maintains a nanosheet structure even under dilute conditions [53]. Moreover, because the T_m of DPPC is 41 °C, which is above room temperature, DPPC membranes form a less fluid gel phase under ambient conditions [54] that tends to provide kinetically stable assemblies. Finally, Chol-TEG-C_5 has a low CMC (< 0.5 mM) as a result of the introduction of hydrophobic end-cap groups, such that dissociation from the edges of the DPPC membranes is suppressed [55]. Consequently, a mixture of DPPC and Chol-TEG-C_5 ([DPPC]/[Chol-TEG-C_5] = 1/5, 5.0 wt% total concentration) was found to generate a clear dispersion without large aggregates even after dilution to 0.2 wt% (Fig. 4d). The ^{31}P NMR spectra acquired from such dispersions exhibited a negative peak shift derived from the orientation of the DPPC/Chol-TEG-C_5 nanosheets over the concentration range of 0.2–5.0 wt% (Fig. 4e). Furthermore, TEM images confirmed the formation of nanosheets with diameters ranging from 200 nm to 2 μm (Fig. 4f, g).

Because the T_m of DPPC (41 °C) is close to body temperature (37 °C), DPPC/Chol-TEG-C_5 nanosheets could potentially be used as a thermoresponsive material capable of undergoing a structural transition from nanosheets to micelles upon heating in the body to facilitate cellular uptake. Indeed, during trials in which DPPC/Chol-TEG-C_5 nanosheets containing the anticancer drug DOX ([DPPC]/[Chol-TEG-C_5] = 5:1 mol/mol, concentration of DOX: 24 μM) were incubated with Hep3B cancer cells at 25 °C, minimal cell death was observed (Fig. 4h, j). Conversely, many dead Hep3B cells containing DOX were observed after incubation at 37 °C (Fig. 4i, k). This temperature-responsive behavior of DPPC/Chol-TEG-C_5 nanosheets could permit the design of transdermal drug delivery systems to be administered near room temperature and activated by body temperature in skin tissue [56].

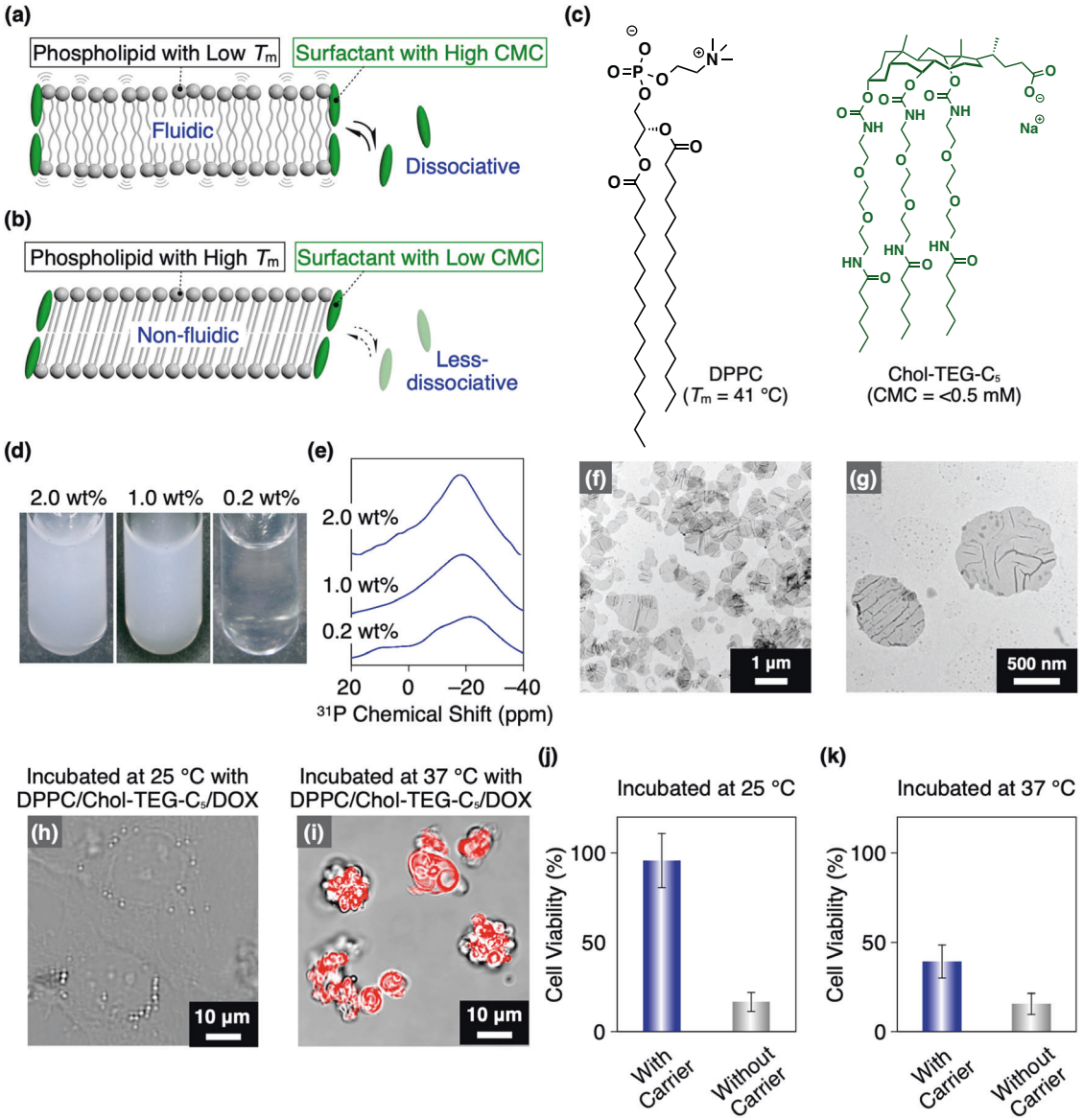

Fig. 4 Diagrams of the structures of (**a**) a conventional nanosheet and (**b**) a kinetically stable nanosheet. Legend: T_m = bilayer melting point, CMC = critical micelle concentration. **c** Molecular structures of the phospholipid DPPC and of Chol-TEG-C_5. **d** Photographic images and (**e**) ^{31}P NMR spectra of aqueous dispersions of DPPC/Chol-TEG-C_5 nanosheet assemblies ([DPPC]/[Chol-TEG-C_5] = 5:1, mol/mol) at concentrations of 2.0, 1.0 and 0.2 wt% and 25 °C. **f** Large-area and (**g**) zoomed-in TEM images of Chol-TEG-C_5 nanosheets deposited on a hydrophilized carbon grid from a 0.04 wt% aqueous dispersion and stained with uranyl acetate. Merged bright-field and fluorescence images of Hep3B cells incubated with 0.1 wt% aqueous dispersions of DPPC/Chol-TEG-C_5/DOX assemblies ([DPPC]/[Chol-TEG-C_5] = 5:1 mol/mol, concentration of DOX: 24 μM) at (**h**) 25 °C (the nanosheet state) and (**i**) 37 °C (the micelle state). These images were acquired during trials involving the in vitro thermoresponsive delivery of DOX to Hep3B cells by DPPC/Chol-TEG-C_5 acting as a carrier. Hep3B cells were incubated with 0.1 wt% aqueous dispersions of DPPC/Chol-TEG-C_5/DOX assemblies ([DPPC]/[Chol-TEG-C_5] = 5:1 mol/mol, concentration of DOX: 24 μM) at various temperatures. Viability of Hep3B cells incubated with DOX (24 μM) at (**j**) 25 °C and (**k**) 37 °C in the presence (blue) or absence (gray) of DPPC/Chol-TEG-C_5 assemblies. Reprinted from [22] with permission from Wiley

Phospholipid nanosheets for blood administration

Phospholipid nanosheets have also been utilized for blood administration based on designing surfactants with higher biocompatibility [23]. In prior work, a cholic acid derivative attached to the metal-binding peptide amino acid sequence PHGGGPHGGG (Chol-MBP; Fig. 5a) was developed as a surfactant and mixed with DPPC ([DPPC]/[Chol-MBP] = 5/1, 5.0 wt% in total) to produce DPPC/Chol-MBP nanosheets. PHGGG is a naturally occurring Cu^{2+} binding motif because of the metal-coordinating ability of the imidazole group of the histidine residues [57]. Because each

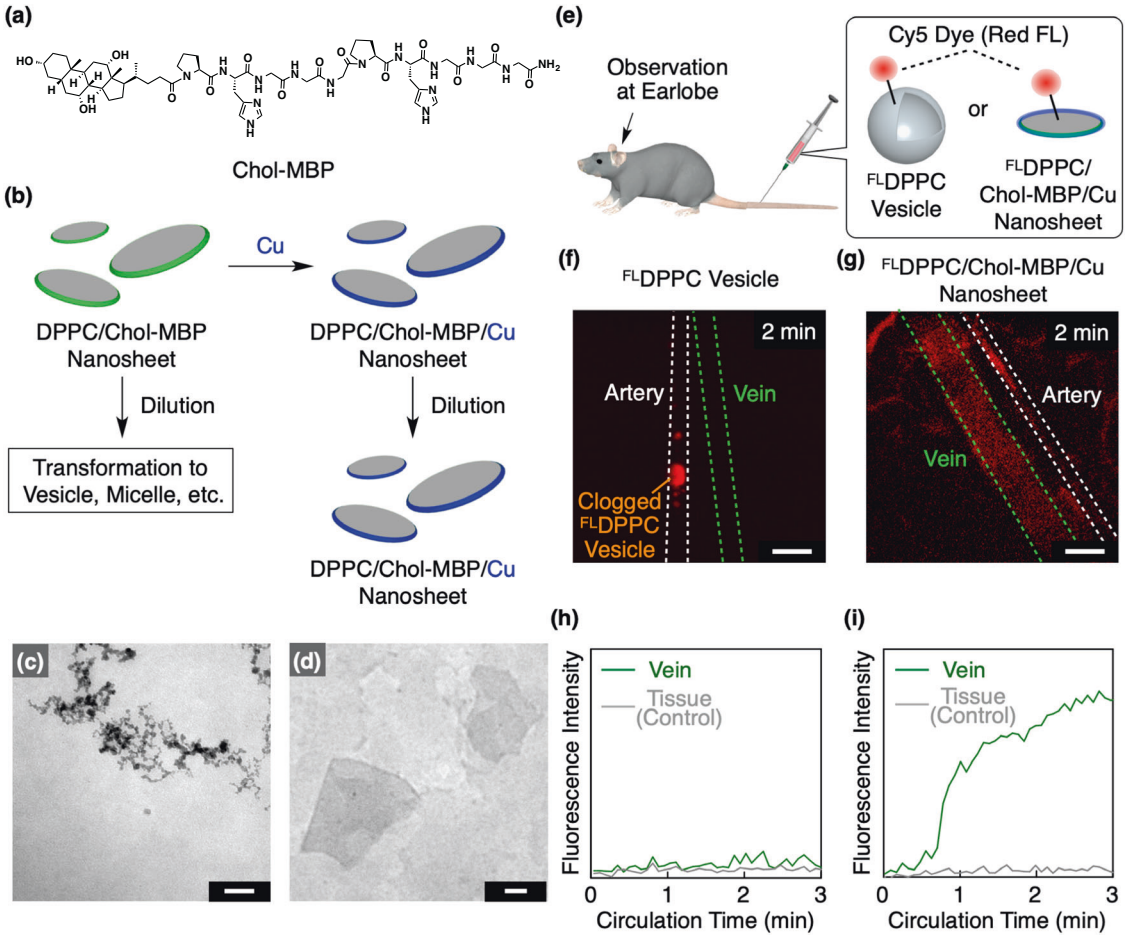

Fig. 5 **a** Molecular structure of Chol-MBP. **b** Diagram showing the preparation of DPPC/Chol-MBP nanosheets and subsequent Cu^{2+}-mediated metal coordination of Chol-MBP to afford crosslinked DPPC/Chol-MBP/Cu nanosheets. After crosslinking, the disk structure of the nanosheets is stable when diluted and in the presence of serum protein. TEM images of mixtures of DPPC and Chol-MBP (total concentration = 0.20 wt%) (**c**) without and (**d**) with 2.0 equiv. Cu^{2+}. Scale bars: 100 nm. **e** Diagram showing the in vivo delivery of ^{FL}DPPC and ^{FL}DPPC/Chol-MBP/Cu nanosheets. IV-CLSM images (λ_{ext} = 640 nm) of blood vessels in a mouse earlobe 2 min after the injection of (**f**) ^{FL}DPPC vesicles (total concentration: 5.0 wt% before injection) and (**g**) ^{FL}DPPC/Chol-MBP/Cu nanosheets (total concentration: 5.0 wt% before injection). Scale bars: 100 µm. Fluorescence intensities over time from trials using (**h**) ^{FL}DPPC vesicles and (**i**) ^{FL}DPPC/Chol-MBP/Cu nanosheets. These fluorescence data were acquired from a vein (green) and tissue (gray) as a control. Reprinted from [23] with permission from the Royal Society of Chemistry

Chol-MBP can bind to two Cu^{2+} ions, these moieties can cross-link at the edges of DPPC/Chol-MBP membranes to inhibit dissociation (Fig. 5c), thus improving the stability of the phospholipid nanosheets. Indeed, when a DPPC/Chol-MBP nanosheet dispersion was diluted to 0.2 wt%, spherical aggregates less than 100 nm in diameter were observed by TEM (Fig. 5c). In contrast, after the addition of 2.0 equiv. of Cu^{2+} ions to afford DPPC/Chol-MBP/Cu nanosheets, the nanosheet structure was maintained after dilution (Fig. 5d). These results indicate that the Cu^{2+}-mediated crosslinking of Chol-MBP significantly improved the stability of these nanosheets in response to dilution.

These structurally stable DPPC/Chol-MBP/Cu nanosheets were used to investigate the effect of the morphology of phospholipid aggregates on the blood circulation profile. For this purpose, fluorescent Cy5-labeled DPPC vesicles and DPPC/Chol-MBP/Cu nanosheets (^{FL}DPPC vesicles and ^{FL}DPPC/Chol-MBP/Cu nanosheets, respectively, total concentration: 5.0 wt% before injection) were prepared, passed through a membrane with 200 nm pores, and then administered to mice via the tail vein. Confocal laser scanning microscopy observations of the earlobes of the mice (IV-CLSM) were performed to evaluate blood circulation (Fig. 5e). The IV-CLSM data confirmed that the ^{FL}DPPC vesicles tended to aggregate and clog blood vessels (Fig. 5f). Fluorescence data acquired over time indicated minimal transfer of these vesicles from the artery to the vein (Fig. 5h). In sharp contrast, ^{FL}DPPC/Chol-MBP/Cu nanosheets were homogeneously dispersed in the blood vessels (Fig. 5g), and the time course of fluorescence monitoring revealed prolonged circulation of this material (Fig. 5i). Hence, it was demonstrated that phospholipid

nanosheets exhibited longer circulation in blood than spherical vesicles. Therefore, it is likely that stabilized phospholipid nanosheets could be a suitable carrier for delivery to the whole body by blood administration.

Conclusion and future perspectives

There has recently been significant progress in the study of nanosheets and supramolecular polymers, leading to the development of supramolecular nanosheets as a new trend integrating these two concepts. Although supramolecular nanosheets have had limited applications due to their structural instability, recent advances in nanotechnology have made it possible to create several more stable versions of these nanosheets. The author previously developed supramolecular nanosheets composed of tubulin protein and phospholipid membranes that exhibited unique functions. These prior studies clearly demonstrated that supramolecular nanosheets are promising next-generation materials that can be designed to produce various structural motifs.

Acknowledgements The author acknowledges the support of a Grant-in-Aid for Early-Career Scientists (JP19K15378) together with funding from the Japan Association for Chemical Innovation, the Moritani Foundation, the Tanaka Foundation, the Kose Cosmetology Foundation, the Konica Minolta Foundation, the Izumi Foundation, the Asahi Glass Foundation and the Iketani Foundation.

Compliance with ethical standards

Conflict of interest The author declares no competing interests.

References

1. Mas-Ballesté R, Gómez-Navarro C, Gómez-Herrero J, Zamora F. 2D materials: To graphene and beyond. Nanoscale. 2011;3:20–30.
2. Deng D, Novoselov KS, Fu Q, Zheng N, Tian Z, Bao X. Catalysis with two-dimensional materials and their heterostructures. Nat Nanotechnol. 2016;11:218–30.
3. Zhao M, Huang Y, Peng Y, Huang Z, Ma Q, Zhang H. Two-dimensional metal-organic framework nanosheets: Synthesis and applications. Chem Soc Rev. 2018;47:6267–95.
4. Mendoza-Sánchez B, Gogotsi Y. Synthesis of two-dimensional materials for capacitive energy storage. Adv Mater. 2016;28:6104–35.
5. Osada M, Sasaki T. Two-dimensional dielectric nanosheets: Novel nanoelectronics from nanocrystal building blocks. Adv Mater. 2012;24:210–28.
6. Aida T, Meijer EW, Stupp SI. Functional supramolecular polymers. Science. 2012;335:813–7.
7. Brunsveld L, Folmer BJB, Meijer EW, Sijbesma RP. Supramolecular polymers. Chem Rev. 2001;101:4071–97.
8. Webber MJ, Appel EA, Meijer EW, Langer R. Supramolecular biomaterials. Nat Mater. 2015;15:13–26.
9. Yan X, Wang F, Zheng B, Huang F. Stimuli-responsive supramolecular polymeric materials. Chem Soc Rev. 2012;41:6042–65.
10. Yashima E, Ousaka N, Taura D, Shimomura K, Ikai T, Maeda K. Supramolecular helical systems: Helical assemblies of small molecules, foldamers, and polymers with chiral amplification and their functions. Chem Rev. 2016;116:13752–990.
11. Davis R, Berger R, Zentel R. Two-dimensional aggregation of organogelators induced by biaxial hydrogen-bonding gives supramolecular nanosheets. Adv. Mater. 2007;19:3878–81.
12. Nam KT, Shelby SA, Choi PH, Marciel AB, Chen R, Tan L, et al. Free-floating ultrathin two-dimensional crystals from sequence-specific peptoid polymers. Nat Mater. 2010;9:454–60.
13. Mannige RV, Haxton TK, Proulx C, Robertson EJ, Battigelli A, Butterfoss GL, et al. Peptoid nanosheets exhibit a new secondary-structure motif. Nature. 2015;526:415–20.
14. Hughes M, Xu H, Frederix PWJM, Smith AM, Hunt NT, Tuttle T, et al. Biocatalytic self-assembly of 2D peptide-based nanostructures. Soft Matter. 2011;7:10032–8.
15. Suzuki Y, Cardone G, Restrepo D, Zavattieri PD, Baker TS, Tezcan FA. Self-assembly of coherently dynamic, auxetic, two-dimensional protein crystals. Nature. 2016;533:369–73.
16. Gonen S, DiMaio F, Gonen T, Baker D. Design of ordered two-dimensional arrays mediated by noncovalent protein-protein interfaces. Science. 2015;348:1365–8.
17. Sinclair JC, Davies KM, Vénien-Bryan C, Noble MEM. Generation of protein lattices by fusing proteins with matching rotational symmetry. Nat Nanotechnol. 2011;6:558–62.
18. Fukui T, Kawai S, Fujinuma S, Matsushita Y, Yasuda T, Sakurai T, et al. Control over differentiation of a metastable supramolecular assembly in one and two dimensions. Nat Chem. 2017;9:493–9.
19. Evans CG, Winfree E. Physical principles for DNA tile self-assembly. Chem Soc Rev. 2017;46:3808–29.
20. Alberstein R, Suzuki Y, Paesani F, Tezcan FA. Engineering the entropy-driven free-energy landscape of a dynamic nanoporous protein assembly. Nat Chem. 2018;10:732–9.
21. Uchida N, Kohata A, Okuro K, Cardellini A, Lionello C, Zizzi EA, et al. Reconstitution of microtubule into GTP-responsive nanocapsules. Nat Commun. 2022;13:5424.
22. Uchida N, Horimoto NN, Yamada K, Hikima T, Ishida Y. Kinetically stable bicelles with dilution tolerance, size tunability, and thermoresponsiveness for drug delivery applications. Chem BioChem. 2018;19:1922–6.
23. Takagi Y, Uchida N, Anraku Y, Muraoka T. Stabilization of bicelles using metal-binding peptide for extended blood circulation. Chem Commun. 2022;58:5164–7.
24. Uchida N, Yanagi M, Hamada H. Bicelle composed of 1,2-dipalmitoyl-sn-glycero-3-phosphatidylcholine and sodium cholate. Nat Prod Commun. 2022;17:1–4.
25. Dürr DHN, Gildenberg M, Ramamoorthy A. The magic of bicelles lights up membrane protein structure. Chem Rev. 2012;112:6054–74.
26. Desai A, Mitchison TJ. Microtubule polymerization dynamics. Annu Rev Cell Dev Biol. 1997;13:83–117.
27. Yajima H, Ogura T, Nitta R, Okada Y, Sato C, Hirokawa N. Conformational changes in tubulin in GMPCPP and GDP-taxol microtubules observed by cryoelectron microscopy. J Cell Biol. 2012;198:315–22.
28. Wang HW, Long S, Finley KR, Nogales E. Assembly of GMPCPP-bound tubulin into helical ribbons and tubes and effect of colchicine. Cell Cycle. 2005;4:1157–60.
29. Zhang R, Alushin GM, Brown A, Nogales E. Mechanistic origin of microtubule dynamic instability and its modulation by EB proteins. Cell. 2015;162:849–59.
30. Mitchison T, Kirschner M. Dynamic instability of microtubule growth. Nature. 1984;312:237–42.
31. Kerssemakers JWJ, Munteanu EL, Laan L, Noetzel TL, Janson ME, Marileen D. Assembly dynamics of microtubules at molecular resolution. Nature. 2006;442:709–12.

32. Hoenger A, Sablin EP, Vale RD, Fletterick RJ, Milligan RA. Three–dimensional structure of a tubulin–motor–protein complex. Nature. 1995;376:271–4.
33. Shaw RJ, Cantley LC. Ras, PI(3)K and mTOR signalling controls tumour cell growth. Nature. 2006;441:424–30.
34. Hsu NY, Ilnytska O, Belov G, Santiana M, Chen YH, Takvorian PM, et al. Viral reorganization of the secretory pathway generates distinct organelles for RNA replication. Cell. 2010;141:799–811.
35. Meshkini A. Fine-tuning of the cellular signaling pathways by intracellular GTP levels. Cell Biochem Biophys. 2014;70:27–32.
36. Kruse AC, Ring AM, Manglik A, Hu J, Hu K, Eitel K, et al. Activation and allosteric modulation of a muscarinic acetylcholine receptor. Nature. 2013;504:101–6.
37. Lin J, Gagnon MG, Bulkley D, Steitz TA. Conformational changes of elongation factor G on the ribosome during tRNA translocation. Cell. 2015;160:219–27.
38. van Dijk AA, Makeyev EV, Bamford DH. Initiation of viral RNA-dependent RNA polymerization. J Gen Virol. 2004;85:1077–93.
39. Walsh D, Mohr I. Viral subversion of the host protein synthesis machinery. Nat Rev Microbiol. 2011;9:860–75.
40. Kumar M, Jayaram H, Carpio RVD, Jiang X, Taraporewala ZF, Jacobson RH, et al. Crystallographic and biochemical analysis of rotavirus NSP2 with nucleotides reveals a nucleoside diphosphate kinase-like activity. J Virol. 2007;81:12272–84.
41. Hu B, Guo H, Zhou P, Shi ZL. Characteristics of SARS-CoV-2 and COVID-19. Nat Rev Microbiol. 2020;19:141–54.
42. Inaoka T, Ochi K. RelA protein is involved in induction of genetic competence in certain Bacillus subtilis strains by moderating the level of intracellular GTP. J Bacteriol. 2002;184:3923–30.
43. Otero AS. NM23/nucleoside diphosphate kinase and signal transduction. J Bioenerg Biomembr. 2000;32:269–75.
44. Smee DF, Hurst BL, Egawa H, Takahashi K, Kadota T, Furuta Y. Intracellular metabolism of favipiravir (T-705) in uninfected and influenza A (H5N1) virus-infected cells. J Antimicrob Chemother. 2009;64:741–6.
45. Sharma A, Sharma US. Liposomes in drug delivery: Progress and limitations. Int J Pharm. 1997;154:123–40.
46. Bozzuto G, Molinari A. Liposomes as nanomedical devices. Int J Nanomed. 2015;10:975–99.
47. Marcotte I, Auger M. Bicelles as model membranes for solid- and solution-state NMR studies of membrane peptides and proteins. Concepts Magn Reson Part A. 2005;24:17–37.
48. Muro S, Garnacho C, Champion JA, Leferovich J, Gajewski C, Schuchman EH, et al. Control of endothelial targeting and intracellular delivery of therapeutic enzymes by modulating the size and shape of ICAM-1-targeted carriers. Mol Ther. 2008;16:1450–8.
49. Doshi N, Prabhakarpandian B, Rea-Ramsey A, Pant K, Sundaram S, Mitragotri S. Flow and adhesion of drug carriers in blood vessels depend on their shape: A study using model synthetic microvascular networks. J Control Release. 2010;146:196–200.
50. Adriani G, de Tullio MD, Ferrari M, Hussain F, Pascazio G, Liu X, et al. The preferential targeting of the diseased microvasculature by disk-like particles. Biomaterials. 2012;33:5504–13.
51. Barbosa-Barros L, Rodríguez G, Barba C, Cócera M, Rubio L, Estelrich J, et al. Bicelles: Lipid nanostructured platforms with potential dermal applications. Small. 2012;8:807–18.
52. Mineev KS, Nadezhdin KD, Goncharuk SA, Arseniev AS. Characterization of small isotropic bicelles with various compositions. Langmuir. 2016;32:6624–37.
53. Beaugrand M, Arnold AA, Hénin J, Warschawski DE, Williamson PTF, Marcotte I. Lipid concentration and molar ratio boundaries for the use of isotropic bicelles. Langmuir. 2014;30:6162–70.
54. Matsuki H, Goto M, Tada K, Tamai N. Thermotropic and barotropic phase behavior of phosphatidylcholine bilayers. Int J Mol Sci. 2013;14:2282–302.
55. Lu Z, Van Horn WD, Chen J, Mathew S, Zent R, Sanders CR. Bicelles at low concentrations. Mol Pharm. 2012;9:752–61.
56. Nakamura K. Central circuitries for body temperature regulation and fever. Am J Physiol Regul Integr Comp Physiol. 2011;301:R1207–R1228.
57. Ghosh S, Verma S. Metalated peptide fibers derived from a natural metal-binding peptide motif. Tetrahedron Lett. 2007;48:2189–92.

Noriyuki Uchida received his BSc from Keio University in 2010. He obtained his PhD under the supervision of Prof. Takuzo Aida from the University of Tokyo in 2015. After working as a postdoctoral fellow at the RIKEN Center for Emergent Mater Science, he was appointed as an assistant professor at Tokyo University of Agriculture and Technology. His current study is focused on supramolecular materials using biomacromolecules.